Translational Science

Cancer Research

Identification of a Small Molecule That Selectively Inhibits ERG-Positive Cancer Cell Growth

Ahmed A. Mohamed[1], Charles P. Xavier[1], Gauthaman Sukumar[2], Shyh-Han Tan[1], Lakshmi Ravindranath[1], Nishat Seraj[3], Vineet Kumar[4], Taduru Sreenath[1], David G. McLeod[1], Gyorgy Petrovics[1,5], Inger L. Rosner[1,5,6], Meera Srivastava[2,5], Jeffrey Strovel[7], Sanjay V. Malhotra[4], Nicole A. LaRonde[3], Albert Dobi[1,5], Clifton L. Dalgard[2,5], and Shiv Srivastava[1,5]

Abstract

Oncogenic activation of the ETS-related gene (*ERG*) by recurrent gene fusions (predominantly TMPRSS2–ERG) is one of the most validated and prevalent genomic alterations present in early stages of prostate cancer. In this study, we screened small-molecule libraries for inhibition of ERG protein in *TMPRSS2–ERG* harboring VCaP prostate cancer cells using an In-Cell Western Assay with the highly specific ERG-MAb (9FY). Among a subset of promising candidates, 1-[2-Thiazolylazo]-2-naphthol (NSC139021, hereafter ERGi-USU) was identified and further characterized. ERGi-USU selectively inhibited growth of ERG-positive cancer cell lines with minimal effect on normal prostate or endothelial cells or ERG-negative tumor cell lines. Combination of ERGi-USU with enzalutamide showed additive effects in inhibiting growth of VCaP cells. A screen of kinases revealed that ERGi-USU directly bound the ribosomal biogenesis regulator atypical kinase RIOK2 and induced ribosomal stress signature. *In vivo*, ERGi-USU treatment inhibited growth of ERG-positive VCaP tumor xenografts with no apparent toxicity. Structure-activity–based derivatives of ERGi-USU recapitulated the ERG-selective activity of the parental compound. Taken together, ERGi-USU acts as a highly selective inhibitor for the growth of ERG-positive cancer cells and has potential for further development of ERG-targeted therapy of prostate cancer and other malignancies.

Significance: A highly selective small-molecule inhibitor of ERG, a critical driver of early stages of prostate cancer, will be imperative for prostate cancer therapy. *Cancer Res; 78(13); 3659–71.* *©2018 AACR.*

Introduction

Cancer of the prostate (CaP) is estimated to be the most frequently diagnosed non-skin malignancy and second leading cause of cancer-related deaths in 2018 among men in the United States (1). Currently, early detected organ confined CaP is managed by active surveillance, surgery, or radiotherapy (2). A significant subset of patients with CaP (20%–40%) experience biochemical recurrence after definitive treatment, prompting hormone ablation and chemotherapy (3). Despite initial response, CaPs often become resistant to therapy, for which there is no effective treatment to date. New AR axis inhibitors (abiraterone and enzalutamide) are leading to significant improvements in treatment of castration-resistant prostate cancer (CRPC; refs. 4–7). Similar to other cancers, discovery of CaP driver genes is providing new opportunities in development of targeted therapy (8–10). Thus, the molecular stratification of the CaP is increasingly critical for enhancing CaP treatment.

Oncogenic activation of *ERG* represents an early CaP driver event and, therefore, it is a promising therapeutic target toward the early targeted treatment of CaP (11). Inhibition of ERG at early stages of the disease may halt the emergence of progression-associated genomic alterations characteristic to the genomic landscape of advanced, largely untreatable disease (12). Recurrent *TMPRSS2–ERG* gene fusions present in nearly half of all CaP in Western countries, resulting in male hormone-dependent and tumor cell–specific expression of the ERG protooncogene and oncoprotein (11). Rare *ERG* gene fusions, including *EWS–ERG* and *TLS/FUS–ERG*, were originally reported in a subset of Ewing sarcoma and leukemia, respectively (13, 14). *ERG* overexpression has also been recognized in myelogenous leukemia (AML; ref. 15). The ERG expression as endothelial cell–specific marker was noted in virtually all vascular tumors, including Kaposi sarcoma (16, 17). Thus, there is a broader potential utility of ERG-targeted therapies. ERG transcription factor is expressed in the natural context of endothelial cells, including blood and lymphatic vessels, where it plays an essential gatekeeper role in the renewal

[1]Center for Prostate Disease Research, Department of Surgery, Uniformed Services University of the Health Sciences and the Walter Reed National Military Medical Center, Bethesda, Maryland. [2]Department of Anatomy, Physiology and Genetics, Uniformed Services University of Health Sciences, Bethesda, Maryland. [3]Department of Chemistry and Biochemistry, University of Maryland, College Park, Maryland. [4]Division of Radiation & Cancer Biology, Department of Radiation Oncology, Stanford University School of Medicine, Stanford, California. [5]John P. Murtha Cancer Center, Walter Reed National Military Medical Center, Bethesda, Maryland. [6]Urology Service, Walter Reed National Military Medical Center, Bethesda, Maryland. [7]Noble Life Sciences, Gaithersburg, Maryland.

Note: Supplementary data for this article are available at Cancer Research Online (http://cancerres.aacrjournals.org/).

A.A. Mohamed and C.P. Xavier contributed equally to this article.

Corresponding Authors: Shiv Srivastava, Center for Prostate Disease Research, Bethesda, MD 20814. Phone: 240-453-8952; Fax: 240-453-8912; E-mail: ssrivastava@cpdr.org; and Clifton L. Dalgard, Department of Anatomy, Physiology and Genetics, Collaborative Health Initiative Research Program, Uniformed Services University of the Health Sciences, Bethesda, MD 20814. Phone: 301-295-1970; E-mail: clifton.dalgard@usuhs.edu

doi: 10.1158/0008-5472.CAN-17-2949

of endothelial cells (16, 17). Therefore, systemic targeting of ERG requires high selectivity for ERG-positive cancer cells with no or minimal effect on normal endothelial cells. Early investigations, including ours, have demonstrated that knockdown of ERG by siRNAs could lead to growth inhibition of *TMPRSS2–ERG*-positive VCaP prostate cancer cells in both cell culture and in tumor xenograft models (18, 19). The emerging strategies to inhibit ERG include direct as well as indirect targeting of ERG (20–32). The ERG-targeted therapies include inhibition of the DNA-binding and transcription activator function of ERG, destabilization of ERG protein, inhibition of CaP-associated *ERG* mRNA, blocking direct ERG interacting coactivators, or the simultaneous disruption of cooperating ERG upstream and downstream factors or its downstream signaling events, including NF-κB or NOTCH (21–32).

Taken together, ERG oncoprotein and the ERG network represent promising, however challenging targets for ERG-positive CaP and other cancers. We and others have reported earlier therapeutic potential of inhibiting ERG in CaP cells (18, 19).

Although an increasing number of studies continues to stress the development of direct or indirect ERG inhibitors, further investigations are warranted (33). We report here the identification and characterization of a small molecule that is a highly selective inhibitor for the growth of ERG-positive cancer cells with no/minimal effect on endothelial cells in *in vitro* and *in vivo*.

Materials and Methods

Cell lines

Human tumors derived cell lines (VCaP, COLO320, KG-1, MOLT4, LNCaP, and MDAPCa2b) were obtained from the ATCC and were grown in cell culture medium and conditions recommended by the supplier. Cell cultures of normal tissue origins [primary cultures of human umbilical vein endothelial cells (HUVEC), and RWPE-1 cell line, adult normal prostate tissue–derived epithelial cells immortalized with human papillomavirus-18] were also obtained from the ATCC. All the cell lines obtained from the ATCC are routinely authenticated and tested for *Mycoplasma* contamination by the vendor using short tandem repeat (STR) profiling kit (cat. #135-XV) and Universal Mycoplasma Detection Kit (cat. #30-1012K). Each cell line was passaged fewer than 6 months after resuscitation. BPH-1 cell line derived from benign prostatic hyperplasia epithelial cell cultures immortalized with SV40 large T-antigen was kindly provided by Dr. Simon Hayward (Vanderbilt University Medical Center, Nashville, TN) and maintained in RPMI 1640 medium supplemented with 5% fetal bovine serum (FBS). LAPC4, a metastatic prostate cancer cell line, was kindly provided by Dr. Charles Sawyer (then at UCLA, Los Angeles, CA) and was grown in IDMD medium with 15% FBS. The LAPC-4 and BPH-1 cell lines were not authenticated due to the absence of available reference database.

Reagents

The mouse monoclonal anti-ERG antibody (9FY) was developed and characterized by our center (16, 34, 35) that is available through Biocare Medical Inc. Antibodies against the androgen receptor (AR; sc-816), glyceraldehyde phosphate dehydrogenase (GAPDH; sc-25778), and α-tubulin (sc-5286) were from Santa Cruz Biotechnology. Antibody for prostate-specific antigen (PSA; A0562012) was from Dako. Antibody sampler kits for measuring apoptosis (9915S) and cell cycle (9932S) were purchased from Cell Signaling Technology. Anti-phospho-S6RP(cat. #2211), anti-S6RP(cat. #2217), and anti-mTOR (cat. #2983) antibodies were also from Cell Signaling Technology. RIOK2 mouse monoclonal antibody (TA505140) was purchased from Origene. Sheep anti-mouse IgG-HRP (NXA931) and donkey-anti rabbit IgG-HRP (NXA934V) were from GE Health Care. The Approved Oncology Drugs Set, Diversity Set II, Mechanistic Set and Natural Products Set small-molecule libraries were obtained from the Developmental Therapeutics Program (DTP) of the National Cancer Institute (http://dtp.nci.nih.gov/branches/dscb/repo_open.html). The 1-[2-Thiazolylazo]-2-naphthol (ERGi-USU) was also obtained from Sigma-Aldrich. Z-VAD-FMK was obtained from Promega. The AR inhibitors bicalutamide and enzalutamide (MDV3100) were purchased from Selleckchem.

Screening of small-molecule compounds by monitoring ERG oncoprotein in an In-Cell Western assay platform

To identify inhibitor small-molecule compounds that lead to decreases in ERG protein levels, a collection of 2,407 small-molecules library consisting of diverse chemical scaffolds, which includes natural products and approved oncology drugs from National Cancer Institute's diversity set, was used in the primary screen. We used the 9FY antibody to measure the response of ERG oncoprotein levels to treatments with small-molecule compounds in an In-Cell Western assay (LI-COR Biosciences). VCaP cells were plated at 20,000 cells per well in 96-well plate and allowed to recover for 12 hours before exposure to 1 μmol/L of the small-molecule library compounds for a period of 48 hours. Cells were briefly washed, fixed with paraformaldehyde, permeabilized, immunolabeled with the primary antibody (9FY), washed, and were stained with Sapphire700 (non-vital cell stain), DRAQ5 (DNA stain), and secondary conjugated IRDye 800CW Goat anti-Mouse IgG (H + L). Plates were scanned and imaged on a Li-COR Odyssey Imager. Values for ERG protein levels detected by IRDye 800 fluorescence intensities and cell density detected by Sapphire700, DRAQ5 was normalized by well position on the 96 well plates. Ratio of normalized ERG expression signal values and cell count signal values was used to detect candidate compounds with the cutoff value that were greater than 2.0 SDs from the mean ratio values. The screen was performed in technical duplicates at different time points and positive candidate hit compounds consistently greater than the cutoff value were selected. Representative images of VCaP cells exposed to the lead compound 1-[2-Thiazolylazo]-2-naphthol for 24 and 48 hours are shown (Supplementary Fig. S1A and S1B).

ERG and *RIOK2* Inhibition by siRNAs

Transfection of cells with siRNA was performed as previously reported (19). Nontargeting (NT; D-001206-13-20), *ERG*-specific small interfering RNA (siRNA) oligo duplexes (5′ CGACAUCCUUCUCUCACAU 3′: si-1; or 5′ UGAUGUUGAUAAAGCCUUA 3′: si-2) against human *ERG* gene (gene ID: 2078; accession: NM_004449) were purchased from GE Healthcare Dharmacon. Two siRNAs were used to minimize off target or nonspecific effect of the siRNAs for *ERG* knockdown. Because both siRNAs showed identical results, si-1 was used in subsequent experiments for ERG (Supplementary Fig. S1C–S1E). Human *RIOK1*-specific On-Target plus SMARTpool RNA (siRNA; 5′ CCAAUAAUGCUAAGAAGUC 3′, 5′ GGAGGCGUGUAUAUCAUUG 3′, 5′ GAACAUGGAUGCUUAUCUC 3′, 5′ GCGCCAACGUCAAUGAUUU 3′) against human *RIOK1* gene (gene ID: Q9BRS2; Uniprot),

RIOK2-specific On-Target plus SMARTpool RNA (siRNA; 5′ UGGGAGCUAUGAAUCAGUA 3′, 5′ GUCCAGGGCUAUCGGUUGA 3′, 5′ CCAGAUGGGUGUUGGCAAA 3′, 5′ UGAAGGAAUUUGCCUAUAU 3′) against human *RIOK2* gene (gene ID: Q9BVS4; Uniprot) and *RIOK3*-specific On-Target plus SMARTpool RNA (siRNA; 5′GCUGAAGGACCAUUUAUUA 3′, 5′GCAGGAAUGUCUCGCAGUU 3′, 5′ UUAAAGAUCGCUUCAGUAA 3′, 5′ GAAAGGAGUCUGUUGUCUU 3′) against human *RIOK3* gene (gene ID: BOYJ89,B4E1Q4, O14730; Uniprot). Cells were cultured in their respective growth medium for 48 hours followed by transfection with 25 or 50 nmol/L of NT siRNA or si-1-*ERG* or *RIOK1,2,3* siRNA using Lipofectamine 2000 (Invitrogen).

Characterization of the compound candidates for the inhibition of ERG protein levels and ERG-associated functions

To evaluate the inhibition of ERG protein levels and its downstream effects, cells were treated for indicated time and dosage of small molecules and were lysed in Mammalian Protein Extraction Reagent (M-PER; Thermo Fisher) containing protease inhibitor cocktail and phosphatase inhibitor cocktails II and III (Sigma). Fifty micrograms of protein from cell lysates was separated through 4% to 12% Bis–Tris Gel (Invitrogen) and transferred to PVDF membrane (Invitrogen). Membranes were first incubated at 4°C for 12 hours with primary antibodies for ERG, AR, PSA, and GAPDH and then washed with wash buffer three times for 5 minutes each at room temperature, followed by incubation with relevant secondary antibodies for 1 hour at 24°C. Finally, membranes were washed three times and developed with ECL Western blot detection reagent (GE Healthcare). To assess cell growth, monolayer of adherent cells were grown in their respective medium for 48 hours followed by treatment with indicated dosage and time for the small-molecule inhibitor. The medium was replaced every 24 hours containing the same concentration of the small-molecule compound. Cells were counted by using the trypan blue exclusion method. Cell morphology was documented by photography in all indicated time points. IC_{50} was calculated using GraphPad Prism 6 software (www.graphpad.com). For quantitative measurement of mRNA levels, total RNA was isolated by using TRIzol (Invitrogen) and RNeasy Mini Kit (Qiagen).

Evaluation of ERGi-USU in prostate tumor xenograft models

Procedures involving mice were approved by the Institutional Animal Care and Use Committee at the Uniformed Services University of Health Sciences in compliance with the Guide for the Care and Use of Laboratory Animals. Male athymic nude mice (6–8 weeks old and weighing 27–30 g) were obtained from The Charles River Laboratory. The VCaP prostate cancer cell line harboring *TMPRSS2–ERG* fusion were trypsinized and washed twice with ice-cold PBS, and were resuspended in ice-cold 50% matrigel in serum-free DMEM medium. A total of 4×10^6 cells/0.1 mL/mouse were subcutaneously injected into the lower right dorsal flank of the mice. Prior to injection, mice were anesthetized with inhalation anesthesia (isoflurane). Tumor growth was monitored weekly after injection. Three weeks after injection, when tumors were palpable, mice were randomly separated into 2 experimental groups and into one control group of 6 mice in each group. In the treatment groups, mice were injected intraperitoneally with 100 mg/kg of ERGi-USU or 150 mg/kg of ERGi-USU, while the control group was injected with vehicle (1:1[v/v], DMSO/PEG300) only. Growth in tumor volume was recorded weekly by using digital calipers, and tumor volumes were calculated by using the $1/2$ ($L \times W2$) formula, where L is the length of tumor and W is the width. Tumor volumes were compared between treated and control groups with repeated measurements. Mice were euthanized at 26 days of treatment. Prior to the experiments, subtoxic doses of ERGi-USU were determined based on the publicly available data (https://dtp.cancer.gov), where a range between 12.5 and 400 mg/kg was used for toxicity assay in mice. Further, we tested sublethal doses from 25 to 250 mg/kg and determined 150 mg/kg as the effective dose using ERGi-USU as (1:1[v/v], DMSO/PEG300) for intraperitoneal injections.

Identification of direct ERGi-USU targets by KINOMEscan screening platform

To identify ERGi-USU targets potentially regulating ERG, we used high-throughput (HTP) screening of 456 kinases from human kinome using site-directed ligand competition binding assay in two independent experiments (KINOMEscan and DiscoverX). In this assay, the dose-dependent competition of the ERGi-USU against immobilized active site ligands with DNA-tagged kinases was measured. The ability of ERGi-USU to compete with the immobilized ligands was monitored by qRT-PCR amplifying the DNA tag.

Expression and purification of human RIOK2 and the filamentous fungus *Chaetomium thermophilum* Riok2

Full-length human RIOK2 (HsRIOK2) was expressed as a recombinant protein in *Escherichia coli*. Briefly, a plasmid vector, pET27b+ (encoding HsRIOK2 tagged with an N-terminal 6×His tag and tobacco etch virus) protease cleavage site, was transformed into Rosetta (DE3) PLysS cells (Novagen). Single colonies were used to inoculate overnight cultures grown in kanamycin containing LB media at 37°C. Large-scale cultures were inoculated by dilution of the overnight culture 1:100 LB media containing 50 μg/mL kanamycin and grown at 37°C. Protein expression was induced at mid-log phase, and cultures were transferred to 20°C for 12 to 16 hours. The cells were harvested by centrifugation and stored at −80°C until purification. Cell pellets were resuspended in buffer containing 100 mmol/L Tris pH 8.0, 500 mmol/L NaCl, 10% glycerol, 0.2% β-mercaptoethanol, 2.5 mmol/L $MgCl_2$, 50 μg/mL DNAse I, and 10 μg/mL RNAse A (50 mL per 1 L culture). Chemical lysis was performed by adding 10 μg/mL of Lysozyme and 2 to 4 mL of Bugbuster (Novagen) while stirring on ice for 45 minutes. The soluble fraction of the lysate was obtained by ultracentrifugation at 25,000 RPM in a Beckman 45 Ti rotor, and the lysate was passed over a 0.22-μm filter prior to affinity purification using a HisTrap column (GE Healthcare Life Sciences). Purified protein was dialyzed into 50 mmol/L Tris pH 8.0, 500 mmol/L NaCl, 10% glycerol, and 0.2% β-mercaptoethanol and concentrated for storage at −80°C. Full-length *Chaetomium thermophilum* RioK2 (CtRiok2) was purified as described previously (36).

Confirmation of ERGi-USU binding to RIOK2 by tryptophan fluorescence quenching assay

For HsRIOK2, the buffer containing 50 mmol/L Tris pH 8.0, 500 mmol/L NaCl, 10% glycerol, and 2.5 mmol/L $MgCl_2$ was used. The ERGi-USU compound was dissolved into 50% DMSO in buffer. One microliter of serial dilutions of the molecule in 50% DMSO was added to 150 μL of buffer containing 4 μmol/L HsRIOK2 for the measurements. The blank sample contained

150 μL buffer plus 1 μL 50% DMSO. For CtRiok2, the buffer used was 50 mmol/L Tris pH8.0, 200 mmol/L NaCl, 10% glycerol, 2.5 mmol/L $MgCl_2$, and the protein concentration was 2 μmol/L. All other reaction conditions were the same as for HsRIOK2. Emission spectra were collected of the blank, protein only, and protein plus ERGi-USU at varying concentrations after excitation at 295 nm. The blank was used to correct for buffer background by subtraction from the sample spectra. Each scan is an average of 10 measurements.

Generation of ERGi-USU derivatives by structure–activity relationship

To identify ERGi-USU derivatives with similar activity and to address ERG selectivity and potential off-target activity of the compound, a total of 134 derivatives with substitutions for key structural and physicochemical properties such as alkyl, alkoxy, cycloalkyl, heterocycloalkyl, aryl, heteroaryl, or hydroxyl groups considering structure–activity relationship (SAR) were commercially obtained or designed and synthesized. Target selectivity and therapeutic efficacy of the new derivatives were evaluated for both ERG-positive and ERG-negative cell lines.

Statistical analysis

Statistical significance of the results between two groups of experiments was defined by Students *t* test and was expressed in *P* values.

Results

Small-molecule library screening for ERG inhibitors by In-Cell Western platform identified ERGi-USU as a potent ERG inhibitor

ETS transcription factor family members, including ERG, show remarkable similarities in their DNA binding and transcriptional activation domain structure. However, there is a clear distinction in their biological functions in differentiation and homeostasis (37). Thus, we reasoned that selective inhibition of ERG expression may be achieved by small molecules. For the inhibition of endogenous ERG protein levels in *TMPRSS2–ERG* fusion–positive prostate cancer cell line (VCaP), we utilized a highly specific anti-ERG mouse monoclonal antibody, 9FY, in an In-Cell Western assay platform. A collection of 2,407 small molecules was used in the primary screen (Fig. 1A and B). Thirty-four candidate compounds were identified, which exhibited decreased ERG protein levels with greater than 2.0 SDs in two independent experiments (Fig. 1B). One compound was observed to significantly increase the ERG protein expression, and upon decoding it was found to be a synthetic androgen. This observation is consistent with the androgen-responsive function of the *TMPRSS2* gene promoter (38), fused to *ERG* in the context of *TMPRSS2–ERG* gene rearrangement in CaP (11).

Ten of the 34 candidate compounds demonstrated variable dose-dependent effects and minimal cell toxicity during a secondary screen for cell viability. To further assess the screening results, these 10 selected ERG inhibitors were also analyzed for ERG mRNA levels by qRT-PCR (Supplementary Table S1; Supplementary Figs. S1F and S2). Based on the inhibition of ERG protein and mRNA, the ERGi-USU was identified as the lead compound and was subjected for in-depth evaluation (Fig. 1B, inset; Supplementary Fig. S3). Using ERG-positive VCaP cells, the IC_{50} for ERGi-USU was defined for cell growth (IC_{50} = 169 nmol/L) and ERG protein (IC_{50} = 315 nmol/L) inhibition (Fig. 1C and D).

Selective inhibition of ERG-positive cancer cells by ERGi-USU

To evaluate the ERG selectivity of the ERGi-USU, a panel of the following cell lines was assessed: ERG-positive tumor cell lines (prostate cancer: VCaP; colon cancer: COLO320; leukemia: KG-1, MOLT-4; ERG negative prostate cancer cell lines (LNCaP, LAPC4, MDA PCa2b); normal prostate epithelium-derived cell lines (BPH-1, RWPE-1); and primary endothelium derived cells (HUVEC). Among these, only ERG-positive cancer cells (VCaP, COLO320, KG-1, and MOLT-4) exhibited dose- and time-dependent inhibition of cell growth in response to ERGi-USU (Fig. 2A and B). ERG protein levels were reduced in VCaP cell line that harbors a 32-amino acid N-terminal truncated ERG protein and in the full-length ERG expressing COLO320, KG-1, and MOLT-4 cell lines. In contrast to malignant ERG-harboring cells, ERG-negative cancer cell lines or normal prostate or endothelium-derived cells were refractory to the cell growth–inhibitory effect of ERGi-USU. Importantly, ERG protein levels were unaffected in normal primary endothelium-derived HUVEV cells. The IC_{50} of ERGi-USU for cell growth inhibition of responsive cell lines ranged between 30 and 400 nmol/L, in contrast to IC_{50} of over 10 μmol/L for nonresponsive cells, suggesting for its high therapeutic index (Fig. 2A; Supplementary Table S2; Supplementary Fig. S4).

Because ERG expression in the *TMPRSS2–ERG* context is AR dependent, we also evaluated the effect of ERGi-USU on AR and its downstream target PSA in hormone-responsive prostate cancer cell lines. With the exception of AR/ERG-positive VCaP cells, the AR and PSA expressions were not affected in any of the AR-positive/ERG-negative CaP cell lines, including LNCaP, LAPC4, and MDA PCa 2b (Supplementary Fig. S5). Overall, the AR-independent action of ERGi-USU was also supported by its growth-inhibitory effect on AR-negative/ERG-positive tumor cell lines (COLO320, MOLT4, and KG1).

Evaluation of a combination of ERGi-USU and AR inhibitors on CaP cell growth

Because both ERG and androgen axis alterations are common drivers of CaP tumorigenesis, we evaluated potential synergy of ERGi-USU with two widely used AR inhibitors, bicalutamide and enzalutamide used following the failure of systemic hormonal ablation. We treated VCaP or LNCaP cells with varying doses of ERGi-USU alone or in combination with AR inhibitors. An additive effect of ERGi-USU and the enzalutamide was noted on VCaP cell growth with linear reduction in enzalutamide dosages. For example, combination of 0.5 μmol/L of ERGi-USU with 1 μmol/L of enzalutamide reduced the growth of VCaP cells by over 80% in comparison with the individual treatments of 0.5 μmol/L of ERGi-USU (50%) or by 1 μmol/L enzalutamide (20%; Supplementary Fig. S6A). As expected from previous observations (Supplementary Fig. S4), this additive effect on VCaP cell growth was not apparent in the ERG-negative CaP cell lines (Supplementary Fig. S6B).

ERGi-USU inhibits ERG-positive VCaP xenografts

The major concern in developing ERG inhibitors is the expression and normal homeostatic function of ERG in endothelial cells, including blood and lymphatic vessels. Thus, the *in vivo* demonstration that ERGi-USU has no/minimal effect in mice was critical for further evaluation of ERGi-USU. Moreover, ERGi-USU

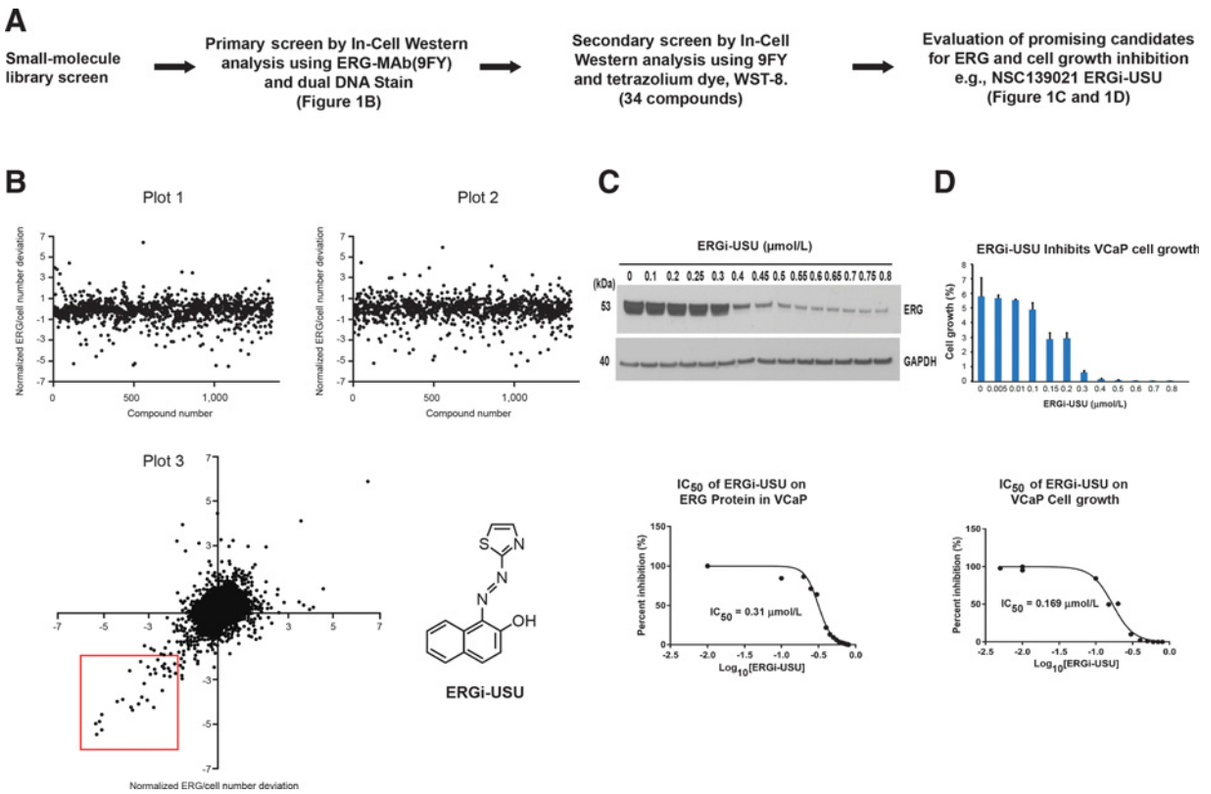

Figure 1.

Small-molecule library screening for identification of inhibitors of the ERG oncoprotein expression. **A,** Screening strategy for the identification of ERGi-USU. **B,** Identification of candidate compounds in small-molecule library primary screen for modulation of ERG protein expression. VCaP cells were plated overnight and then exposed to library compounds for 48 hours. After exposure, cells were briefly washed, fixed before immunolabeling with ERG MAb, and stained with Sapphire700/DRAQ5 dyes for cell density determination. Values were normalized to well position on the plate, and the ratio of ERG signal to cell density was used to determine compound activity on ERG expression. Two individual replicates of the primary screen are shown (plot 1, first screen; plot 2, second screen; plot 3, combined results for normalized ERG expression values of two independent replicates of the primary screen). Positive candidate compounds were identified by the decreased ratio values of at least 2.0 SDs in the two independent technical replicates of the screen. The *Z*-score for the assay was 0.587. SDs for positive and negative control wells were 0.010 and 0.019, respectively, with mean effect size of 0.213. Chemical structure of the lead compound ERGi-USU selected for further characterization is shown in the inset. **C** and **D,** Dose–response curve of ERGi-USU on VCaP cells and IC_{50} determination. **C,** VCaP cells were treated with the indicated concentrations of ERGi-USU for 48 hours to determine the IC_{50} for ERG protein inhibition. **D,** The IC_{50} of VCaP cell growth inhibition at day 8 is shown as cell growth (%) and percentage of inhibition.

is anticipated to reduce the tumor burden in mice harboring ERG-positive prostate tumor xenografts. Toward assessing the antitumorigenic effects of ERGi-USU, and to investigate the potential side effects, including the normal function of ERG in endothelial cells, we examined the effects of ERGi-USU in mice harboring ERG-positive VCaP tumor xenografts. Preestablished tumors of *TMPRSS2–ERG* harboring VCaP xenografts were assessed for tumor growth inhibition in nude mice for 100 mg/kg and 150 mg/kg dosages. No apparent toxicity, including weight loss, lethargy, diarrhea, loss of appetite, respiratory distress, or overall drug-related toxicity, was observed. Gross examination of major organs also revealed no damage in tissues and vasculature as a result of the compound administration. In rare events, localized inflammation at the site of injection was observed at 150 mg/kg dosage. In comparison with the control group (1856.1 mm^3), significant ($P < 0.05$ and $P < 0.005$) inhibition of tumor growth was noted at day 26 in treatment groups (100 mg/kg: 1047.74 mm^3; 150 mg/kg: 654.18 mm^3), indicating 44% and 65% reduction of tumor burden (Fig. 3A and B). Similar observations were made in two additional independent experiments (Supplementary Fig. S7). These data support the *in vivo* efficacy and selectivity of ERGi-USU for ERG-positive prostate cancers.

ERGi-USU directly binds and inhibits RIOK2 protein

The reliance of cancer cells on a specific signaling pathway have been widely documented and known as "oncogenic addiction." We reasoned that the narrow selectivity of ERGi-USU for ERG-positive cancer cells could be traced to a specific kinase controlling both ERG protein stability and transcription in the context of ERG-positive cancer cells. We performed screening of 456 kinases of the human kinome by ligand competition KINOMEscan. In this assay, ERGi-USU competes with the immobilized ligand for binding to the respective kinase conjugated to a DNA tag monitored by quantitative PCR. In each reaction, 12 concentrations of ERGi-USU were used to determine the dissociation constant (K_d) for all 456 kinases in two independent experiments. The assay identified RIOK2 with highest affinity (Kd = 200 nmol/L) to ERGi-USU (Fig. 4A). The resulting affinity of ERGi-USU to RIOK2 was

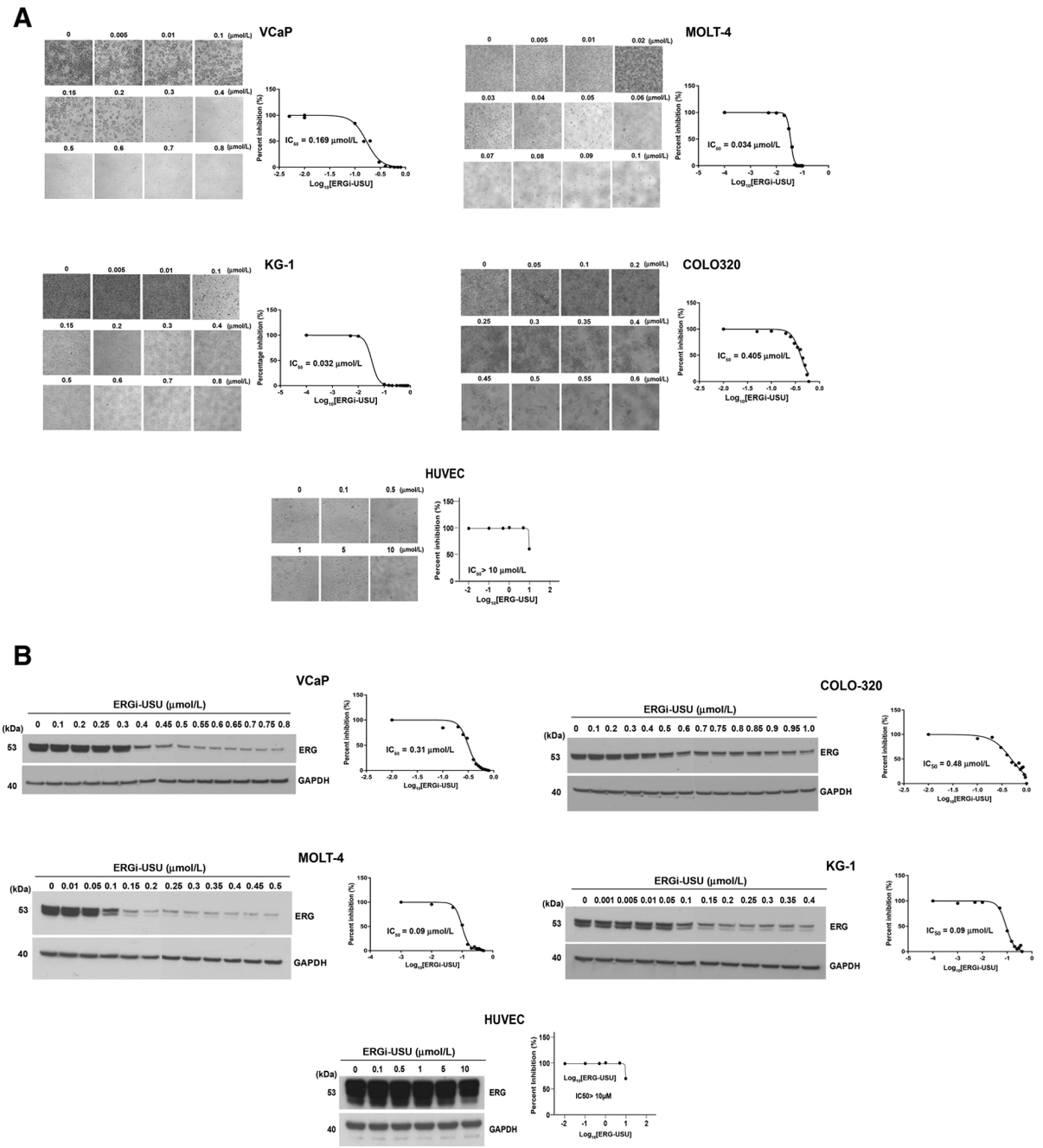

Figure 2.

Assessment of ERGi-USU in a panel of ERG-positive cancer cell lines and normal endothelial cells. **A,** Selective inhibition of ERG-positive cancer cells in cell culture models. Cells were incubated for 8 days with indicated concentrations of ERGi-USU. Cells were trypsinized and counted by using a hemacytometer and trypan blue staining and pictures of representative view fields were taken for each dosage. The IC_{50} values for inhibition of ERG-positive tumor cell growth are shown for each cell line. The cell growth of the ERG-positive primary normal endothelial derived cells (HUVEC) was minimally affected at the highest concentration (10 μmol/L). **B,** ERG-positive tumor cells (VCaP, MOLT4, KG1, and COLO 320) or HUVEC were plated (2×10^6) in 10-cm culture dishes and treated with the indicated concentrations of ERGi-USU for 48 hours. Cell lysates were analyzed for ERG and GAPDH proteins by Western blot assay. The IC_{50} values for ERG protein inhibition are shown for each tested cell line.

strikingly similar to the VCaP cell growth-inhibitory effect of ERGi-USU (IC_{50} = 169 nmol/L). ERGi-USU affinities to other kinases ranked from second to eighth (K_d = 1,300 nmol/L to 3,000 nmol/L) indicated 6- to 10-fold lower affinities and over two orders of magnitude lower affinities to the mean of all other kinases. Thus, the affinity of RIOK2 for ERGi-USU is distinctively higher than all other kinases. RIOK2 is an atypical serine/threonine kinase required for the normal maturation of the 40S subunit of the eukaryotic

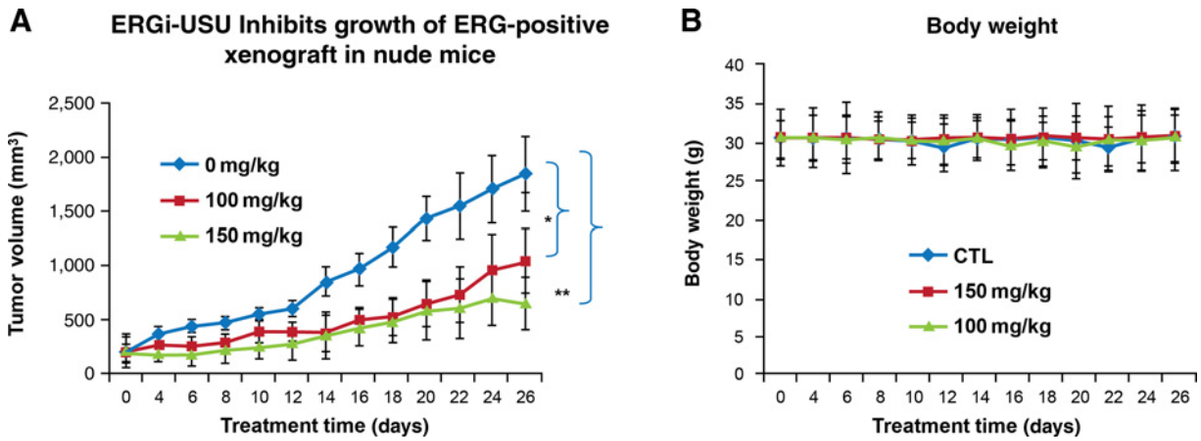

Figure 3.

Selective inhibition of ERG-positive cancer cells by ERGi-USU *in vivo*. **A,** VCaP xenografts were established by subcutaneously injecting cells in male nude mice and grown until tumors were palpable (treatment time = 0). Tumor growth inhibition was assessed at 100 and 150 mg/kg dosages of ERGi-USU, with three treatments per week. Control group received vehicle only. Treatment of ERGi-USU exhibited significant tumor growth inhibition (44% and 65% tumor burden reduction) in comparison with control group. Mean ± SD are shown; *, $P < 0.05$; **, $P < 0.005$. **B,** There was no apparent difference in body weight between treatment groups and the control.

ribosome in ribosomal biogenesis (39). Elevation of ribosomal biogenesis is a required mechanism for proliferating malignant cells. To assess the biological effect of ERGi-USU with its target RIOK2, a panel of ERG-positive tumor cell lines (VCaP and COLO320), ERG-negative tumor cell line (LNCaP), and ERG-positive primary endothelium derived cells (HUVEC) was assayed with standardized doses of ERGi-USU. After 48 hours of treatment, the IC_{50} values for RIOK2 protein inhibition were between 220 nmol/L (VCaP) and 360 nmol/L (COLO320), in contrast to IC_{50} of over 1,000 nmol/L for cells nonresponsive to ERGi-USU. These results showed that dose-dependent decreases in RIOK2 protein levels in response to ERGi-USU closely mirrored the selective cell growth-inhibitory effect of ERGi-USU (Fig. 4B–E and inset). In the kinome scan assay, we have detected RIOK2 and RIOK3 among the top potential binding targets of ERGi-USU. We performed knockdown experiments targeting individually all RIOK family members that includes RIOK1, RIOK2, and RIOK3. Although these experiments did not yield appreciable inhibition (Supplementary Fig. S8), combined knockdown of RIOK1, RIOK2, and RIOK3 resulted in significantly reduced cell growth and reduction of ERG protein levels (Fig. 4F and G and inset).

ERGi-USU preferentially binds to human RIOK2

In order to confirm binding of ERGi-USU by human RIOK2 (HsRIOK2), we tested the ability of the inhibitor molecule to quench the intrinsic tryptophan fluorescence of the purified enzyme. As shown in Fig. 4H, ERGi-USU is capable of quenching fluorescence of the enzyme in a concentration-dependent manner, across a range of 0.67 to 670 nmol/L (the full range tested). As a positive control, we included a reaction containing 1.3 μmol/L ATP and observed fluorescence quenching similar to that observed for the lowest concentration of ERGi-USU tested. These results confirm that the molecule directly interacts with HsRIOK2. In order to test whether the molecule is capable of binding in a species-specific manner, we tested the ability of ERGi-USU to quench intrinsic fluorescence in purified Riok2 from the ancestral filamentous fungus, *Chaetomium thermophilum* (CtRiok2). No quenching was observed until the ERGi-USU concentration was at 6.7 μmol/L, indicating that CtRiok2 has a much lower affinity for ERGi-USU (Fig. 4I). To estimate the equilibrium dissociation constant for ERGi-USU complex formation with HsRIOK2 and CtRiok2, we used the tryptophan fluorescence quenching assays. For HsRIOK2, we used a two-site binding model that reasonably fit the data with a high-affinity site with a K_d of 64 ± 30 nmol/L and a low-affinity site with a K_d of 49 ± 19 μmol/L. For CtRiok2, the data fitted reasonably well with a one-site binding model, with a K_d of 1.3 ± 0.6 μmol/L. These data indicate that ERGi-USU binds with at least 10-fold higher affinity to HsRIOK2 than to the *C. thermophilum* homolog (Supplementary Fig. S9).

ERGi-USU induces ribosomal stress

The established roles of RIOK2 kinase in ribosomal biogenesis prompted us to examine the signature of ERGi-USU in cancer-associated stress pathways affected in ribosomal biogenesis (36). VCaP cells treated with different doses of ERGi-USU were probed for proteins involved in ribosomal stress (Fig. 5A and B). Further, treatment of ERGi-USU resulted in the cleavage of the apoptosis-associated PARP-1, caspase 3 and 7, as well as inhibition of cell-cycle–associated proteins, such as CDK4 and cyclin D1, and cyclin D3. Induction of apoptosis was further confirmed by TUNEL assay (Supplementary Fig. S10A and S10B). To rule out that the observed stress-associated responses to ERGi-USU were not due to apoptosis and catastrophic cell death and to affirm that ERGi-USU action preceded the apoptosis, the temporal relation between ERG modulation and apoptotic markers was evaluated. Inhibition of ERG was evident at 18 hours, and, as expected, induction of cleaved PARP-1 was followed at 24 hours (Supplementary Fig. S10C). Treatment with the apoptosis inhibitor Z-VAD did not protect inhibition of ERG protein by ERGi-USU molecule (Supplementary Fig. S10D), but rescued treated cells from cell death as anticipated. Further, known CaP-associated kinases such as B-RAF, ERGR, and Src were not affected by ERGi-USU, indicating that ERGi-USU activity is not pleiotropic, but selective for the ribosomal biogenesis (Supplementary S11).

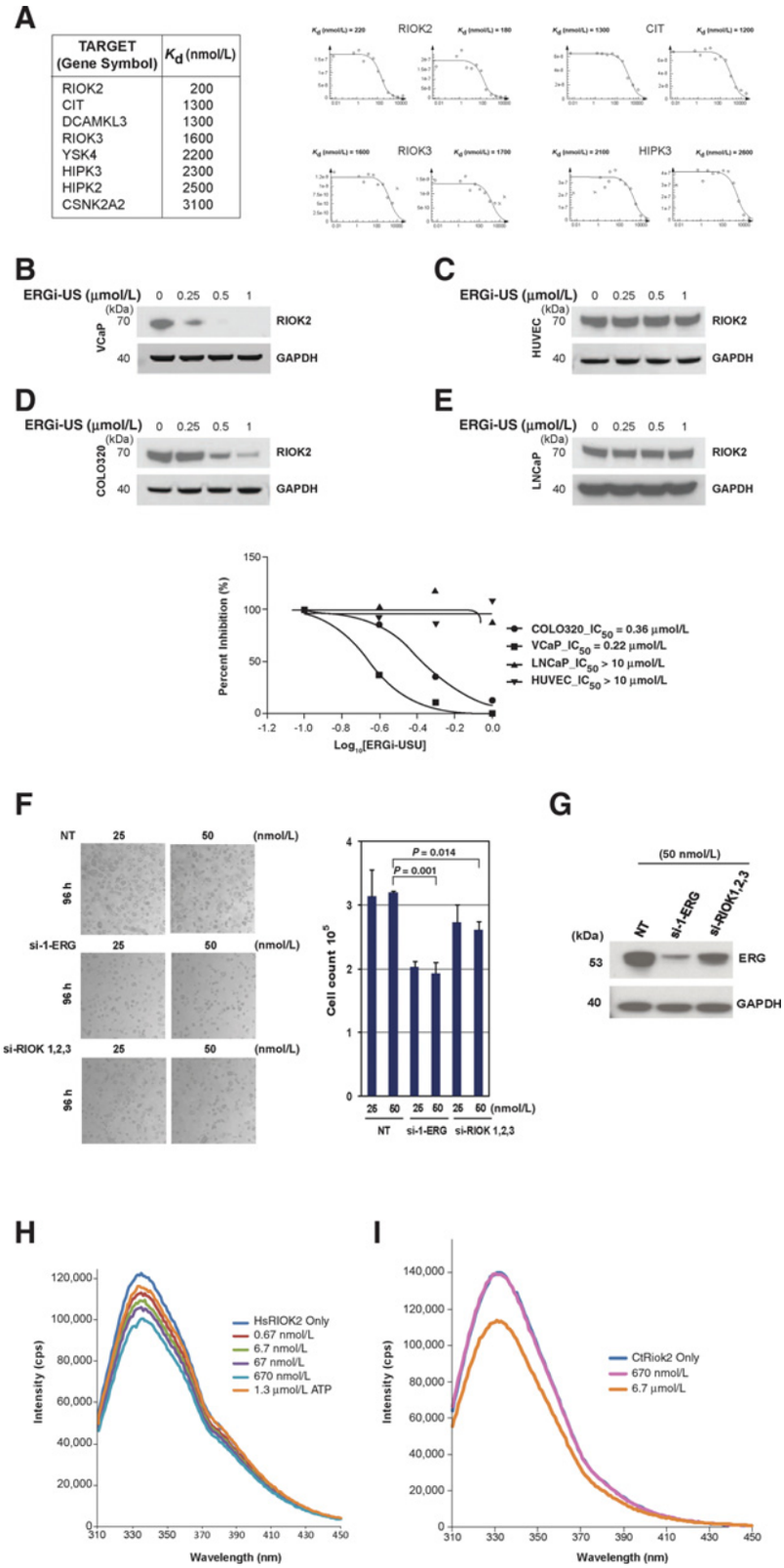

Figure 4.

ERG directly binds and inhibits RIOK2. **A,** Using HTP screening of 456 kinases from human kinome by KINOMEscan, RIOK2 was identified with the highest affinity of Kd = 200 nmol/L. **B–E,** ERGi-USU inhibits RIOK2 proteins in ERG-positive tumor cell lines (VCaP and COLO320) but not in ERG-negative prostate cancer cell line (LNCaP) or ERG-positive normal primary endothelial derived cells (HUVEC). The inset depicts the corresponding IC_{50} values. **F,** Dose-dependent quenching of human RIOK2 (HsRIOK2) tryptophan fluorescence in response to ERGi-USU. **G,** Tryptophan fluorescence quenching of the ancestral Riok2 (CtRiok2) by ERGi-USU was not observed in submicromolar concentrations. **H** and **I,** Combined siRNA-mediated knockdown of RIOK1, RIOK2, and RIOK3 resulted in significant reduction in the growth of VCaP cells (**H**) and reduced ERG protein levels (**I**).

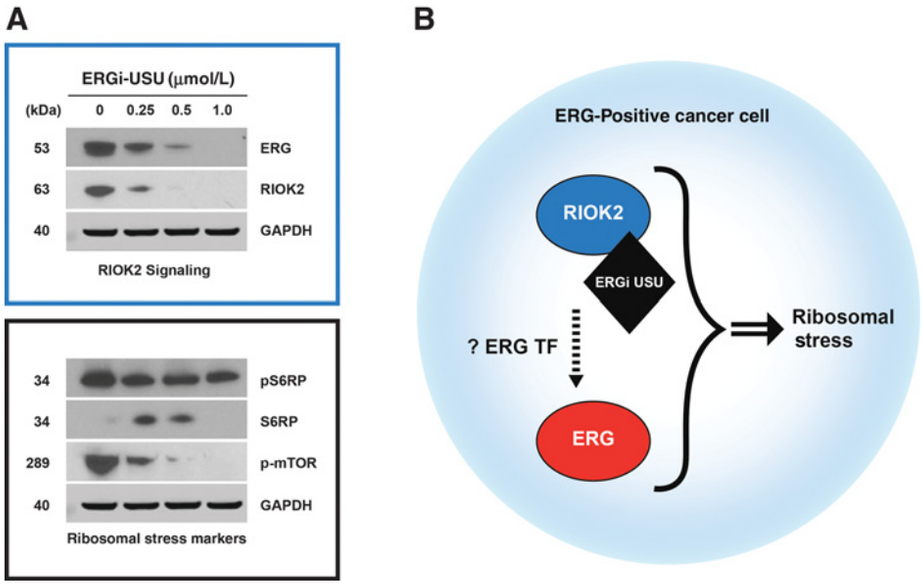

Figure 5.
ERGi-USU induces ribosomal stress signatures. **A,** Treatment of ERGi-USU induces ribosomal stress as indicated by inhibition of RIOK2, pS6RP, S6RP, and mTOR. **B,** We postulate a mechanism of ERGi-USU for selective inhibition of ERG in positive tumor cells. ERGi-USU binds to RIOK2 and inhibits ERG protein levels and transcription through a synthetic lethal interaction with an ERG upstream factor (ERG TF).

Identification of ERGi-USU derivatives (SAR of aza-phenol derivatives as ERG oncogene inhibitors)

We screened a library of 2,407 compounds from National Cancer Institute's diversity set. This library consists of diverse chemical scaffolds and includes natural products and approved oncology drugs. Thiazolyl-diazo-naphthol (parental compound, Fig. 6A) was identified as lead "hit" from this screening showing significant growth inhibition for the ERG-positive VCaP cell line (IC_{50} = 169 nmol/L) and inhibition of ERG protein levels (IC_{50} = 315 nmol/L). We reasoned that the physico-chemical features of this scaffold are responsible for the unexpected ERG-selective growth inhibition of cancer cells. The structure of parental compound consists of (i) thiazoyl ring, (ii) diazo linker, and (iii) naphthol ring (Fig. 6A). Therefore, to improve its efficacy, affirm the ERG selectivity of this class of compounds and establish preliminary SAR, a small set of diazo compounds, were either synthesized or commercially obtained, with modification on these three sites were screened.

Results showed that replacing thiazolyl moiety with phenyl group resulted in complete loss of activity, irrespective of substituents (electron donation or withdrawing) and their position (ortho-, or meta-, or para-) on the phenyl ring. Substitution of the thiazolyl ring with the oxadiazolyl (as shown as A1) or 3-pyridyl (A2) ring also resulted in loss of activity. Interestingly, the derivative with 2-pyridyl (A3) group showed partial activity (IC_{50} = 5,000 nmol/L) toward ERG inhibition. Modification of diazo linker with amine (C1) or amide (C2) groups was also not tolerated. Complete loss of activity was also observed when the naphthol ring was replaced with N-substituted dihydropyrazolone ring (B1 and B2) or phenol ring (B3). Interestingly, compounds with substitution at C-5 position of phenol ring with methyl (B4, IC_{50} = 420 nm) or isopropyl (B5, IC_{50} = 560 nmol/L) showed similar potency for inhibiting ERG protein levels in comparison with the parental compound. In summary, screening results showed a very narrow SAR around parental compound, with all the modification around the thiazolyl ring and diazo linker completely diminished the activity. Taken together, only the compounds where naphthol was replaced with 5-alkyl-substituted phenols showed ERG inhibition activity similar to parental compound (Fig. 6A–C).

Discussion

Oncogenic activation ERG through *TMPRSS2–ERG* fusion is an established recurrent driver gene alteration in early stages of prostate tumorigenesis observed as early as in the preinvasive stages of CaP (4, 11). ERG activation imposes stress mechanisms, setting the stage for destabilization of the CaP genome and selective advantage of cancer cells (40). The causal nature of ERG in prostate and other cancers provides a strong rationale for ERG as a therapeutic target (41–43). Indeed, functional evaluation of *ERG* in CaP suggests that inhibition of *ERG* results in reduced tumor cell growth *in vitro* and *in vivo* (19). Despite the challenges of targeting transcription factors, there have been increasing efforts toward evaluation of direct or indirect inhibitors of ERG (20). Given the impact of ERG oncogenic activation on a large number of patients with cancer, more concerted efforts are warranted toward development of ERG inhibitors. Therapeutic targeting of ERG at early stages of CaP may also lead to earlier pharmacologic interventions similar to successful early treatment of chronic myelogenous leukemia (44).

Along these lines, our strategy for screening small-molecule inhibitors included measurement of intracellular levels of ERG protein in human cell lines. Screening of small-molecule libraries by In-Cell Western assays identified inhibitors of ERG protein levels. A promising compound, ERGi-USU exhibited inhibition of cell growth of ERG-harboring prostate cancer, colon cancer, and leukemia cell lines. In contrast, normal endothelium–derived HUVEC cells and other non-ERG–expressing cell lines did not exhibit measurable response to ERGi-USU. The most striking finding from this study is the virtual exclusivity of ERGi-USU for ERG dependence of ERG-positive tumor cell growth. This unprecedented selectivity was further underscored by the virtual lack of disruption of normal endothelial cells, including blood and lymphatic vessels *in vivo*. To further confirm the ERG selectivity and to enhance the therapeutic efficacy of ERGi-USU, a systematic

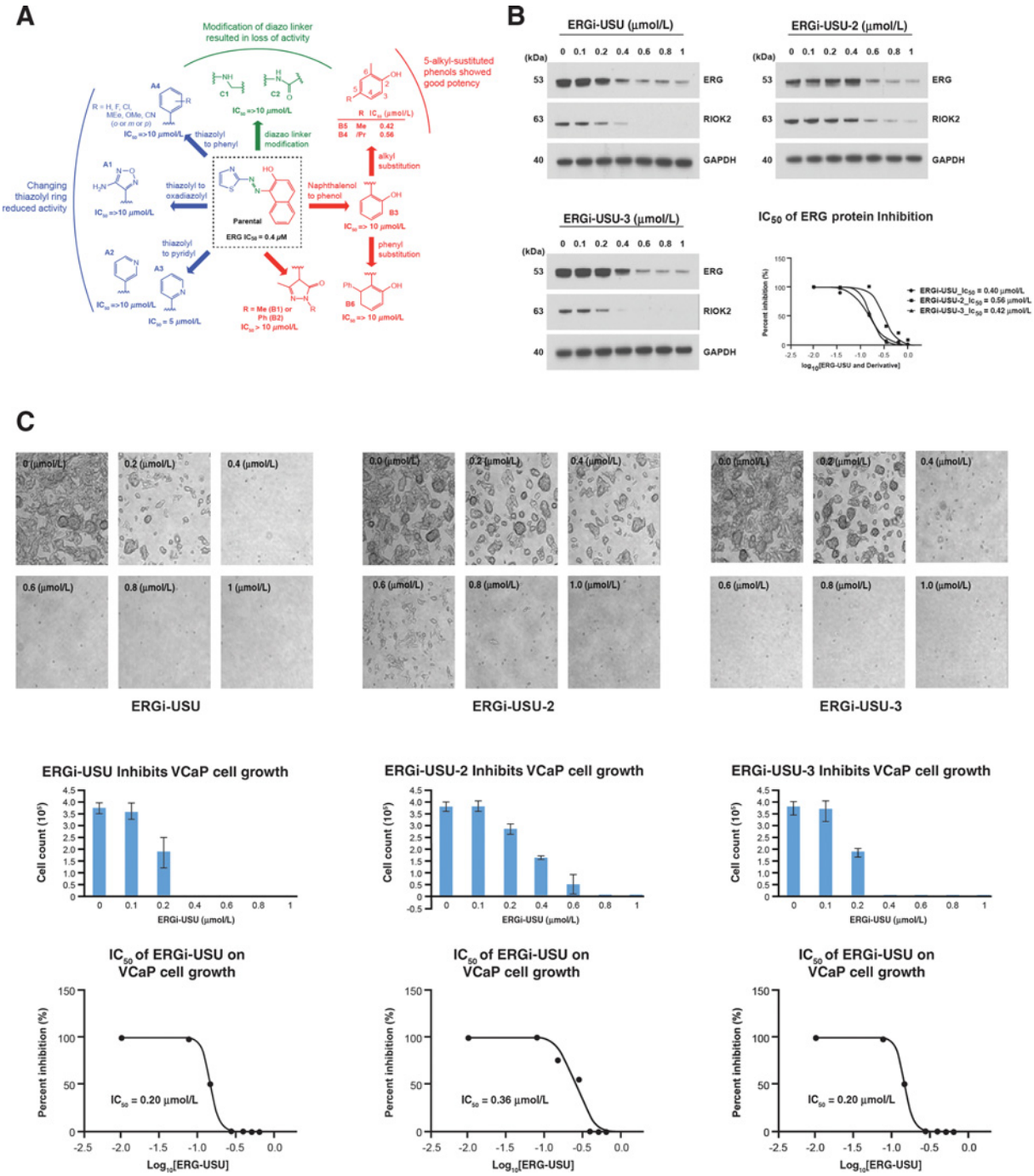

Figure 6.

SAR of aza-phenols for ERG oncogene inhibition. **A,** Compounds where naphthol was replaced with 5-alkyl-substituted phenols showed ERG inhibition activity similar to the parental compound. Structures of modifications around thiazolyl ring or diazo linker of the parental compound resulted in complete loss of activity. **B,** The IC_{50} of ERGi-USU parental and derivatives ERGi-USU-2 and ERGi-USU-3 (are comparable for ERG protein inhibition). **C,** The IC_{50} for cell growth inhibition of ERGi-USU, ERGi-USU-2, and ERGi-USU-3 is also highly similar.

SAR-based approach of ERGi-USU core structure was performed. Two new derivatives with similar activity to the parental compound were identified. The structural analogues were also selective for tumor cell lines that express ERG, indicating ERGi-USU and derivatives are indeed ERG-selective inhibitors. Because the core chemical structural element of ERGi-US selectivity for ERG-positive cancer cells has been defined, focused assessment of further ERGi-USU derivatives are warranted.

Previously six independent experiments were documented by NCI-DTP with NCI-60 cell line panel (http://dtp.nci.nih.gov/branches/dscb/repo_open.html). Among them, MOLT-4 was the only ERG-positive tumor cell line tested. The reported lethal dose (LC_{50}) of NSC139021-(Thiazolylazo-2-naphthol; in this article, ERGi-USU) was between 0.186 and 100 μmol/L in comparison with IC_{50} of 0.034 μmol/L in our MOLT-4 cell growth assay. There has been no previous report of ERG inhibition by ERGi-USU due to the absence of ERG-harboring cell lines in initial screens (45). Although in a chemoprevention context, Brooks et al. also assessed Thiazolylazo-2-naphthol reporting induction of quinone reductase (QR) in HepG2, but no QR response was observed in LNCaP and LNCaPazaC (ERG-negative) cells (45, 46). Of note, *TMPRSS2–ERG* harboring VCaP cell line was not available at that time. Indeed, use of VCaP cells in the current study unraveled the selectivity of ERGi-USU for ERG-positive cancer cells. Initial insights into cell biology–based mechanisms revealed that ERGi-USU directly binds and inhibits the atypical kinase RIOK2 protein with an affinity of 200 nmol/L, that is consistent with the ERG-selective cell growth inhibition of ERGi-USU in ERG-harboring prostate cancer cells (VCaP).

Importantly, in the independent assay of monitoring the dose-dependent tryptophan fluorescence quenching of RIOK2 further substantiated the binding of ERGi-USU to RIOK2. Remarkably, this binding was preferential to the human RIOK2, as opposed to the ancestral eukaryotic Riok2 from a filamentous fungus species. RIOK2 is an integral part of ribosomal biogenesis and it is required for the transport and maturation of the 40S ribosome (36). Inhibition of RIOK2 by ERGi-USU induce ribosomal stress that resembles features of perturbed ribosomal biogenesis, including RIOK2-dependent processes (Fig. 6). ERGi-USU binds to RIOK2 and inhibits levels of ERG and RIOK2 protein in the context of ERG-positive cancer cells, which in turn disrupts ribosomal biogenesis, resulting in ribosomal stress. Consistent with the ribosomal stress signature, we observed phosphorylation of the tumor suppressor p53 at ser15 and inhibition of MDM2, as one of the known mechanisms of p53 activation (Supplementary Fig. S12; Supplementary refs. 1–3). The selective requirement for ERG to facilitate interaction of the ERGi-USU with RIOK2 is intriguing, as in the absence of ERG, ERGi-USU does not affect RIOK2 protein, e.g., in ERG-negative LNCaP cells. The mechanism of the selectivity remains to be better understood. Further, we noted in a kinome screen that RIOK2 and RIOK3 were among the top four kinases ranked by dissociation constants (K_d) for ERGi-USU. Due to potential redundant and compensatory mechanisms between three members of the RIOK family of atypical kinases (RIOK1, RIOK2, and RIOK3), we assessed the growth response of VCaP cells by combined knockdown of RIOK1, RIOK2, and RIOK3. Of note, we observed significant growth inhibition of VCaP cells and reduction in ERG protein levels in these experiments. One of the major limitations of our study is that the interaction of RIOK atypical kinases is not well understood. Thus, further studies are warranted for defining the structural and functional impact of ERGi-USU on RIOKs.

Importantly ERGi-USU significantly inhibited the growth of ERG-positive tumor xenografts in nude mice. Moreover, we did not observed toxicity, consistent with earlier evaluation from NCI-DTP (https://dtp.cancer.gov). Initial mouse toxicity data documented by NCI-DTP for NSC139021(ERGi-USU) reported no toxicity between dosage 12.5 and 400 mg/kg. We used these reference data to design our assay. The lack of toxicity in mouse models is unlikely due to low homology between human and mouse amino acid sequences, because the similarity and identity between mouse and human RIOK2 are 93.5% and 83%, respectively. These reduced to 53% identity and 70.6% similarity for the CtRiok2 protein when compared with HsRIOK2. Further, we believe that ERGi-USU effect is confined to synthetic lethality in the context of ERG-positive cancer cells. Therefore, in this context, one would not expect general toxicity in mice.

This finding further indicated that endothelial cells (HUVEC *in vitro* and mouse *in vivo*), where wild-type ERG is expressed in its natural context, were not affected by ERGi-USU under these experimental conditions. Due to natural expression of ERG in endothelial cells, major conceptual challenge in systemic administration of ERG inhibitors has been related to blood vessel–related toxicity. It is important to note that this, as well as other reports, have not observed such an effect likely due to redundant pathways likely FLI 1 compensating for ERG inhibition in the endothelium. Another promising aspect of the study is the additive effects of ERGi-USU and AR inhibitors for inhibition of ERG-positive prostate cancer cells. Because ERG-positive prostate cancers exhibit better response to androgen ablation therapy (47), the proof of principle *in vitro* data shown here suggest potential of combining AR and ERG inhibitors similar to the combination of hormonal axis and ERG downstream NOTCH inhibitors (31). The mechanism of ERGi-USU induced reduction of AR and PSA selectively in AR-positive VCaP is unclear. However, in AR-negative ERG-positive cell lines (MOLT4 and KG-1), the growth and ERG protein inhibition is clearly independent of AR. The AR effect was not seen in the context of ERG negative but in AR-positive prostate cancer cell lines (e.g., LNCaP and MDAPCa2b). Therefore, the observed AR effect in VCaP is likely due to as yet unidentified parallel mechanisms.

In this report, the observed selectivity of ERGi-USU for only ERG-positive cancer cells offers a unique opportunity in enhancing the further development of ERG-targeted therapeutic approaches. In summary, we have shown that ERGi-USU is a selective inhibitor of ERG-positive tumor cells. This small-molecule inhibitor of ERG exhibited minimal effects on normal endothelial cells. Further efforts to elucidate the mechanism of this high degree of selectivity are warranted.

Disclosure of Potential Conflicts of Interest

J. Strovel is CEO at ConverGene. No potential conflicts of interests were disclosed by the other authors.

Disclaimer

The opinions or assertions contained herein are the private ones of the authors/speakers and are not to be construed as official or reflecting the views of the Department of Defense, the Uniformed Services University of the Health Sciences or any other agency of the U.S. Government.

Authors' Contributions

Conception and design: A.A. Mohamed, C.P. Xavier, M. Srivastava, J. Strovel, A. Dobi, C.L. Dalgard, S. Srivastava

Development of methodology: A.A. Mohamed, C.P. Xavier, J. Strovel, A. Dobi, C.L. Dalgard, S. Srivastava

Acquisition of data (provided animals, acquired and managed patients, provided facilities, etc.): A.A. Mohamed, C.P. Xavier, G. Sukumar, S.-H. Tan, L. Ravindranath, N. Seraj, J. Strovel, N.A. LaRonde, C.L. Dalgard, S. Srivastava

Analysis and interpretation of data (e.g., statistical analysis, biostatistics, computational analysis): A.A. Mohamed, C.P. Xavier, N. Seraj, V. Kumar, T. Sreenath, G. Petrovics, I.L. Rosner, J. Strovel, S.V. Malhotra, N.A. LaRonde, A. Dobi, C.L. Dalgard, S. Srivastava

Writing, review, and/or revision of the manuscript: A.A. Mohamed, C.P. Xavier, S.-H. Tan, D.G. McLeod, I.L. Rosner, S.V. Malhotra, N.A. LaRonde, A. Dobi, C.L. Dalgard, S. Srivastava
Administrative, technical, or material support (i.e., reporting or organizing data, constructing databases): A.A. Mohamed, C.P. Xavier, G. Sukumar, S.-H. Tan, L. Ravindranath, S. Srivastava
Study supervision: J. Strovel, A. Dobi, C.L. Dalgard, S. Srivastava

Acknowledgments

We are grateful to all members of the Center for Prostate Disease Research, Uniformed Services University of Health Sciences, Henry M. Jackson Foundation for the Advancement of Military Medicine, and Stanford Medical School. Special thanks to Dr. Alagarsamy Srinivasan for the guidance and insights in the area of therapeutic molecule development; Mr. Stephen Doyle, CPDR for the art work; Ms. Chantal Falade for administrative support.

This research was supported by the CPDR-USU program HU0001-10-2-0002 to I.L. Rosner, the NCIR01CA162383 grant to S. Srivastava, the USU and HJF Office of Technology TransferFY2015 and FY2016 IP Development Awards to S. Srivastava, and the John P. Murtha Cancer Center Translational Research Fellowship Award to C.P. Xavier.

The costs of publication of this article were defrayed in part by the payment of page charges. This article must therefore be hereby marked *advertisement* in accordance with 18 U.S.C. Section 1734 solely to indicate this fact.

Received October 13, 2017; revised February 13, 2018; accepted April 24, 2018; published first April 30, 2018.

References

1. Siegel RL, Miller KD, Jemal A. Cancer Statistics, 2018. CA Cancer J Clin 2018;68:7–30.
2. Litwin MS, Tan HJ. The diagnosis and treatment of prostate cancer: a review. JAMA 2017;317:2532–42.
3. Facchini G, Perri F, Misso G, D Aniello C, Scarpati GD, Rossetti S, et al. Optimal management of prostate cancer based on its natural clinical history. Curr Cancer Drug Targets 2017. doi: 10.2174/1568009617666170209093101.
4. Tran C, Ouk S, Clegg NJ, Chen Y, Watson PA, Arora V, et al. Development of a second-generation antiandrogen for treatment of advanced prostate cancer. Science 2009;324:787–90.
5. Hung J, Taylor AR, Divine GW, Hafron JM, Hwang C. The effect of time to castration resistance on outcomes with abiraterone and enzalutamide in metastatic prostate cancer. Clin Genitourin Cancer 2016;14:381–8.
6. Brasso K, Thomsen FB, Schrader AJ, Schmid SC, Lorente D, Retz M, et al. Enzalutamide antitumour activity against metastatic castration-resistant prostate cancer previously treated with docetaxel and abiraterone: a multicentre analysis. Eur Urol 2015;68:317–24.
7. Attard G, Belldegrun AS, de Bono JS. Selective blockade of androgenic steroid synthesis by novel lyase inhibitors as a therapeutic strategy for treating metastatic prostate cancer. BJU Int 2005;96:1241–6.
8. Weischenfeldt J, Korbel JO. Genomes of early onset prostate cancer. Curr Opin Urol 2017;27:481–7.
9. Feng FY, Brenner JC, Hussain M, Chinnaiyan AM. Molecular pathways: targeting ETS gene fusions in cancer. Clin Cancer Res 2014;20:4442–8.
10. Cancer Genome Atlas Research Network. The molecular taxonomy of primary prostate cancer. Cell 2015;163:1011–25.
11. Tomlins SA, Rhodes DR, Perner S, Dhanasekaran SM, Mehra R, Sun XW, et al. Recurrent fusion of TMPRSS2 and ETS transcription factor genes in prostate cancer. Science 2005;310:644–8.
12. Robinson D, Van Allen EM, Wu YM, Schultz N, Lonigro RJ, Mosquera JM, et al. Integrative clinical genomics of advanced prostate cancer. Cell 2015;161:1215–28.
13. Ichikawa H, Shimizu K, Hayashi Y, Ohki M. An RNA-binding protein gene, TLS/FUS, is fused to ERG in human myeloid leukemia with t(16;21) chromosomal translocation. Cancer Res 1994;54:2865–8.
14. Sorensen PH, Lessnick SL, Lopez-Terrada D, Liu XF, Triche TJ, Denny CT. A second Ewing's sarcoma translocation, t(21;22), fuses the EWS gene to another ETS-family transcription factor, ERG. Nat Genet 1994;6:146–51.
15. Rao VN, Modi WS, Drabkin HD, Patterson D, O'Brien SJ, Papas TS, et al. The human erg gene maps to chromosome 21, band q22: relationship to the 8; 21 translocation of acute myelogenous leukemia. Oncogene 1988;3:497–500.
16. Miettinen M, Wang ZF, Paetau A, Tan SH, Dobi A, Srivastava S, et al. ERG transcription factor as an immunohistochemical marker for vascular endothelial tumors and prostatic carcinoma. Am J Surg Pathol 2011;35:432–41.
17. Baltzinger M, Mager-Heckel AM, Remy P. Xl erg: expression pattern and overexpression during development plead for a role in endothelial cell differentiation. Dev Dyn 1999;216:420–33.
18. Tomlins SA, Laxman B, Varambally S, Cao X, Yu J, Helgeson BE, et al. Role of the TMPRSS2–ERG gene fusion in prostate cancer. Neoplasia 2008;10:177–88.
19. Sun C, Dobi A, Mohamed A, Li H, Thangapazham RL, Furusato B, et al. TMPRSS2–ERG fusion, a common genomic alteration in prostate cancer activates C-MYC and abrogates prostate epithelial differentiation. Oncogene 2008;27:5348–53.
20. Sedarsky J, Degon M, Srivastava S, Dobi A. Ethnicity and ERG frequency in prostate cancer. Nat Rev Urol 2018;15:125–31.
21. Khemlina G, Ikeda S, Kurzrock R. Molecular landscape of prostate cancer: implications for current clinical trials. Cancer Treat Rev 2015;41:761–6.
22. Brenner JC, Ateeq B, Li Y, Yocum AK, Cao Q, Asangani IA, et al. Mechanistic rationale for inhibition of poly(ADP-ribose) polymerase in ETS gene fusion-positive prostate cancer. Cancer Cell 2011;19:664–78.
23. Asangani IA, Dommeti VL, Wang X, Malik R, Cieslik M, Yang R, et al. Therapeutic targeting of BET bromodomain proteins in castration-resistant prostate cancer. Nature 2014;510:278–82.
24. Fortson WS, Kayarthodi S, Fujimura Y, Xu H, Matthews R, Grizzle WE, et al. Histone deacetylase inhibitors, valproic acid and trichostatin-A induce apoptosis and affect acetylation status of p53 in ERG-positive prostate cancer cells. Int J Oncol 2011;39:111–9
25. Kao CJ, Martiniez A, Shi XB, Yang J, Evans CP, Dobi A, et al. miR-30 as a tumor suppressor connects EGF/Src signal to ERG and EMT. Oncogene 2014;33:2495–503.
26. Wang S, Kollipara RK, Srivastava N, Li R, Ravindranathan P, Hernandez E, et al. Ablation of the oncogenic transcription factor ERG by deubiquitinase inhibition in prostate cancer. Proc Natl Acad Sci U S A 2014;111:4251–6.
27. Wang X, Qiao Y, Asangani IA, Ateeq B, Poliakov A, Cieslik M, et al. Development of peptidomimetic inhibitors of the ERG gene fusion product in prostate cancer. Cancer Cell 2017;31:844–7.
28. Butler MS, Roshan-Moniri M, Hsing M, Lau D, Kim A, Yen P, et al. Discovery and characterization of small molecules targeting the DNA-binding ETS domain of ERG in prostate cancer. Oncotarget 2017;8:42438–54.
29. Rahim S, Beauchamp EM, Kong Y, Brown ML, Toretsky JA, Uren A. YK-4-279 inhibits ERG and ETV1 mediated prostate cancer cell invasion. PLoS One 2011;6:e19343.
30. Shao L, Zhou Z, Cai Y, Castro P, Dakhov O, Shi P, et al. Celastrol suppresses tumor cell growth through targeting an AR-ERG-NF-kappaB pathway in TMPRSS2/ERG fusion gene expressing prostate cancer. PLoS One 2013;8:e58391.
31. Mohamed AA, Tan SH, Xavier CP, Katta S, Huang W, Ravindranath L, et al. Synergistic activity with NOTCH inhibition and androgen ablation in ERG-positive prostate cancer cells. Mol Cancer Res 2017;15:1308–17.
32. Kron KJ, Murison A, Zhou S, Huang V, Yamaguchi TN, Shiah YJ, et al. TMPRSS2–ERG fusion co-opts master transcription factors and activates NOTCH signaling in primary prostate cancer. Nat Genet 2017;49:1336–45.
33. Barbieri CE, Rubin MA. Genomic rearrangements in prostate cancer. Curr Opin Urol 2015;25:71–6.
34. Furusato B, Tan SH, Young D, Dobi A, Sun C, Mohamed AA, et al. ERG oncoprotein expression in prostate cancer: clonal progression of ERG-positive tumor cells and potential for ERG-based stratification. Prostate Cancer Prostatic Dis 2010;13:228–37.
35. Mohamed AA, Tan SH, Mikhalkevich N, Ponniah S, Vasioukhin V, Bieberich CJ, et al. Ets family protein, erg expression in developing and adult mouse tissues by a highly specific monoclonal antibody. J Cancer 2010;1:197–208.

36. Ferreira-Cerca S, Sagar V, Schafer T, Diop M, Wesseling AM, Lu H, et al. ATPase-dependent role of the atypical kinase Rio2 on the evolving pre-40S ribosomal subunit. Nat Struct Mol Biol 2012;19:1316–23.
37. Findlay VJ, LaRue AC, Turner DP, Watson PM, Watson DK. Understanding the role of ETS-mediated gene regulation in complex biological processes. Adv Cancer Res 2013;119:1–61.
38. Nelson PS, Gan L, Ferguson C, Moss P, Gelinas R, Hood L, et al. Molecular cloning and characterization of prostase, an androgen-regulated serine protease with prostate-restricted expression. Proc Natl Acad Sci U S A 1999;96:3114–9.
39. Read RD, Fenton TR, Gomez GG, Wykosky J, Vandenberg SR, Babic I, et al. A kinome-wide RNAi screen in Drosophila Glia reveals that the RIO kinases mediate cell proliferation and survival through TORC2-Akt signaling in glioblastoma. PLos Genet 2013;9:e1003253
40. Sreenath TL, Macalindong SS, Mikhalkevich N, Sharad S, Mohamed A, Young D, et al. ETS related gene mediated androgen receptor aggregation and endoplasmic reticulum stress in prostate cancer development. Sci Rep 2017;7:1109.
41. Klezovitch O, Risk M, Coleman I, Lucas JM, Null M, True LD, et al. A causal role for ERG in neoplastic transformation of prostate epithelium. Proc Natl Acad Sci U S A 2008;105:2105–10.
42. King JC, Xu J, Wongvipat J, Hieronymus H, Carver BS, Leung DH, et al. Cooperativity of TMPRSS2–ERG with PI3-kinase pathway activation in prostate oncogenesis. Nat Genet 2009;41:524–6.
43. Carver BS, Tran J, Gopalan A, Chen Z, Shaikh S, Carracedo A, et al. Aberrant ERG expression cooperates with loss of PTEN to promote cancer progression in the prostate. Nat Genet 2009;41:619–24.
44. Jawhar M, Naumann N, Schwaab J, Baurmann H, Casper J, Dang TA, et al. Imatinib in myeloid/lymphoid neoplasms with eosinophilia and rearrangement of PDGFRB in chronic or blast phase. Ann Hematol 2017;96:1463–70.
45. Brooks JD, Goldberg MF, Nelson LA, Wu D, Nelson WG. Identification of potential prostate cancer preventive agents through induction of quinone reductase in vitro. Cancer Epidemiol Biomarkers Prev 2002;11:868–75.
46. Talalay P, De Long MJ, Prochaska HJ. Identification of a common chemical signal regulating the induction of enzymes that protect against chemical carcinogenesis. Proc Natl Acad Sci U S A 1988;85:8261–5.
47. Ateeq B, Vellaichamy A, Tomlins SA, Wang R, Cao Q, Lonigro RJ, et al. Role of dutasteride in pre-clinical ETS fusion-positive prostate cancer models. Prostate 2012;72:1542–9.